RSC
Applied Interfaces

ROYAL SOCIETY OF CHEMISTRY

COMMUNICATION

View Article Online
View Journal

Cite this: DOI: 10.1039/d5lf00333d

Received 30th October 2025,
Accepted 29th January 2026

DOI: 10.1039/d5lf00333d

rsc.li/RSCApplInter

Endothelial cell adhesion and proliferation on wrinkled diamond-like carbon films on grooved PDMS substrates

So Nagashima, †*[a] Terumitsu Hasebe,†*[b] Atsushi Hotta [c] and Tetsuya Suzuki[c]

Controlling the adhesion and proliferation of endothelial cells is essential for the development of functional vascular materials. In this study, we show that wrinkled diamond-like carbon (DLC) films formed on grooved PDMS substrates regulate endothelial cell alignment and proliferation through combined micro- and nanoscale topographical cues. Human umbilical vein endothelial cells cultured on these hierarchical patterns exhibited directional elongation along the grooves, while their lamellipodia and filopodia preferentially adhered to the wrinkle crests. Enzymatic assays confirmed sustained viability and proliferation across different wrinkle dimensions. These results demonstrate that hierarchical micro-/nanoscale topographies on DLC-coated PDMS substrates can effectively modulate endothelial cell behavior, offering promise for vascular tissue engineering.

Introduction

The integration of biomedical implants with host tissues remains a central challenge in biomedical engineering. Despite significant advances in biomaterial development, clinical outcomes are still hindered by complications such as thrombosis and inflammation. The formation of a continuous and functional endothelial cell layer on implant surfaces is vital because it provides an anti-thrombotic and anti-inflammatory barrier that mitigates these adverse responses.[1] Therefore, the rapid and stable formation of this layer (*i.e.*, endothelialization) is essential; delayed or incomplete coverage can result in device failure, restenosis, or other life-threatening complications. To address these issues, advanced surface modifications and precisely engineered micro- and nanoscale topographies are required that enhance endothelial cell adhesion, proliferation, and function.[2,3]

Microgrooved substrates have been widely used to direct endothelial cell elongation and alignment.[4–8] However, while effective for orienting cells, microgrooves alone often provide limited control over specific adhesion sites that are crucial for focal adhesion formation and robust proliferation. Meanwhile, recent studies have revealed that hierarchical surface structures combining micro- and nanoscale features can synergistically modulate responses of various cells by providing multiple levels of mechanical cues and more closely replicating the architecture of the native extracellular matrix.[9–12] Thus, integrating microgrooves with nanoscale features is considered a rational approach to simultaneously guiding cell alignment and focal adhesion formation, thereby enhancing endothelial proliferation and function. This hierarchical design concept offers a promising route to improve endothelialization on implant surfaces.

In addition to topographical cues, mechanical cues such as substrate stiffness and topographically induced mechanical forces also play a crucial role in regulating endothelial cell behavior. Endothelial cells sense and respond to these mechanical properties of their environment through mechanotransduction pathways involving integrins, focal adhesions, and the cytoskeleton. In particular, substrate stiffness strongly influences cell adhesion, spreading, migration, proliferation, and cytoskeletal organization on substrates that correspond to the physiological stiffness range of the vascular basement membrane and vessel walls.[13] The mechanical mismatch between an implant and the surrounding tissue can impair endothelialization, promote inflammation, and contribute neointimal hyperplasia. Therefore, designing surfaces that combine appropriate stiffness with hierarchical micro-/nanoscale features represents an effective strategy to enhance endothelial function and promote stable implant integration.

Diamond-like carbon (DLC) is a functional coating material having exceptional mechanical, chemical, and

[a] *Department of Mechanical Systems Engineering, Nagoya University, Nagoya 464-8603, Japan. E-mail: so.nagashima@nagoya-u.jp*
[b] *Department of Radiology, Tokai University, Hachioji 192-0032, Japan. E-mail: terumitsuhasebe@tokai.ac.jp*
[c] *Department of Mechanical Engineering, Keio University, Yokohama 223-8522, Japan*
† These authors contributed equally to this work.

biological properties. DLC and its derivatives have thus been extensively studied for industrial and biomedical applications.[14–23] When deposited onto soft polymer substrates, including polydimethylsiloxane (PDMS), DLC films spontaneously develop micro-/nanoscale wrinkles due to mechanical instability arising from strain mismatch between the stiff film and compliant substrate.[24,25] Our previous study established a fabrication method for hierarchical surface patterns combining wrinkled DLC films with microgrooved PDMS substrates.[26] Although these hierarchical patterns present a promising scaffold architecture for endothelialization, their direct influence on endothelial cell adhesion and proliferation has not yet been examined.

In this study, we investigate endothelial behavior on hierarchical patterns composed of wrinkled DLC films formed on grooved PDMS substrates. Using human umbilical vein endothelial cells (HUVECs), we evaluate their attachment, morphology, and proliferation. The results demonstrate that cells tend to align along the groove direction, while lamellipodia and filopodia-like protrusions preferentially attach to wrinkle crests, indicating dual-scale topographical guidance. Enzymatic assays confirm sustained cell viability and proliferation across different wrinkle dimensions, suggesting the noncytotoxic nature of the surfaces. These findings demonstrate that wrinkled and grooved surface topographies cooperatively modulate endothelial cell attachment, elongation, and proliferation, offering a promising surface design for promoting endothelialization on implant materials.

Results and discussion

We begin by describing the surface morphology and chemistry of the patterns using data adapted from our previous study.[26] The pristine grooved PDMS substrate with parallel channels of equal groove and ridge with a width of 5 μm and a depth of 1 μm (Fig. 1a) was treated with Ar plasma for varying durations, followed by deposition of DLC film with a thickness of approximately 40 nm (see SI). This process resulted in the formation of wrinkles aligning perpendicular to the groove steps with varying dimensions depending on the plasma duration (Fig. 1b–e). The formation of these wrinkles results from buckling of the layer produced on the substrate surface due to Ar plasma treatment,[26] while their orientation is attributable to the difference in compressive stress parallel and perpendicular to the groove steps.[27]

The wavelength and amplitude of the wrinkles are plotted as a function of the duration of Ar plasma treatment in Fig. 1f and g. As the plasma duration increased from 1 to 7 min, the wavelength increased from approximately 1017 to 2209 nm, while the amplitude increased from approximately 136 to 210 nm. In film–substrate bilayer systems, both the wavelength and amplitude are functions of the film thickness. Given the constant thickness of the DLC film, the increases in both wavelength and amplitude with longer durations of Ar plasma treatment are attributable to an increase in the thickness of the oxidized layer formed on the substrate surface by the plasma treatment prior to film deposition. Thus, the wrinkle wavelength and amplitude can be controlled simply by adjusting the duration of Ar plasma treatment, while keeping the film thickness constant.

The atomic concentrations for the pattern surfaces before and after DLC coating were measured by X-ray scanning electron microscopy (Fig. 1h). The concentrations of carbon, oxygen, and silicon for the pristine grooved PDMS substrate prior to film coating were approximately 45, 25, and 30 at%, respectively. These values are reasonable because PDMS contains a silicon–oxygen skeleton with two methyl groups attached to the silicon atom with possible surface oxidation or contamination. The increase in the concentration of carbon is attributable to the DLC film because it mainly consists of carbon. The oxygen detected is indicative of the surface oxidation of the film. A small amount of silicon was detected despite the DLC coating, indicating that part of the samples, including the sidewalls of the grooves, was not covered with the film. Overall, the elemental compositions remained nearly constant regardless of the duration of Ar plasma treatment. Consequently, the sample surfaces exhibited distinct hierarchical topographies while maintaining consistent chemistry. We next discuss the viability of the HUVECs on the sample surfaces that was assessed by measuring the enzymatic activity. For these experiments, HUVECs at passage 4 in endothelial basal medium supplemented with endothelial growth factor (EGM-2, Lonza) were seeded on the sample surfaces at a density of approximately 4.6×10^4 cells per mL and were cultured in the incubator for prescribed periods of time in a humidified 5% CO_2 incubator at 37 °C. After prescribed periods, the plates were removed from the incubator, and the medium in each well was replaced with 500 μL of RPMI medium (Lonza) containing 50 μL of Cell Counting Kit-8. The plates were then returned to and placed in the incubator for approximately 90 min. Thereafter, 100 μL of the reaction mixture in each well was transferred to a 96-well plate, and the optical density (OD)—an index of the degree of cellular viability—at 450 nm was measured with a microplate reader (Microplate Reader, EZS ABS, Iwaki Asahi Technoglass).

Fig. 2 shows the OD values measured at 450 nm using the reaction mixture in the wells after periods of 48 and 72 hours. The wells coated with gelatin were used as the positive control to confirm that the cells propagated in a satisfactory manner until the end point of the experiments. The OD values for the positive control increased as the period increased from 48 to 72 hours. These results indicate that the initial seeding cell density was appropriate and that the cells proliferated normally under these conditions. The OD values for the hierarchical patterns were lower than that of the positive control. These lower values are presumably due to the inhibition of adsorption of proteins to the surfaces of DLC films that are involved in the cell adhesion. Despite the initial low OD values for the hierarchical patterns, they all

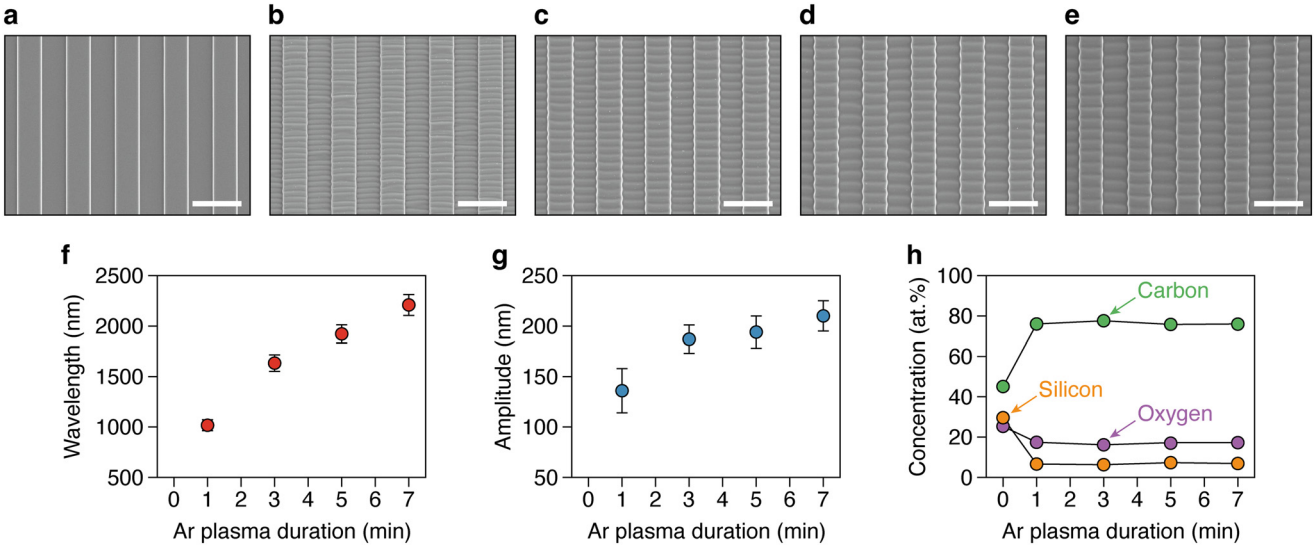

Fig. 1 Surface morphology and chemistry of the patterns. (a–e) SEM images of the surfaces. (a) Pristine grooved PDMS substrate. (b–e) DLC-coated grooved PDMS substrates pre-treated with Ar plasma for varying durations: (b) t = 1 min; (b) t = 3 min; (b) t = 5 min; (b) t = 7 min. Scale bars: 10 μm. (f and g) Wavelength (f) and amplitude (g) of the wrinkles as a function of the duration of Ar plasma pre-treatment. (h) Atomic concentration of the pattern surfaces. Adapted with permission from previous work.[26]

increased toward the end point of the experiments (*i.e.*, 72 hours of culture). These results suggest that the adhesion and proliferation of the HUVECs were retained on the hierarchical patterns, thus indicating their non-cytotoxicity. Although the wavelength and amplitude of the wrinkles were different among the hierarchical patterns, no significant differences were observed in the OD values among the surfaces in the time frame established for the experiment.

In this study, cell viability and proliferation on the wrinkled and grooved surfaces were assessed using the CCK-8 assay, which enables comparative evaluation of cell metabolic activity under identical culture conditions. While this method effectively revealed relative differences in cellular responses among the tested surfaces, additional quantitative analyses would further strengthen the interpretation of the results. Future studies will incorporate additional biological assessments, including fluorescence-based live/dead staining and quantitative correlation between OD values and viable cell number, to obtain a more comprehensive understanding of the effect of wrinkled and grooved patterns on endothelial cell viability and proliferation.

Finally, we describe the cell morphology on the hierarchical patterns examined by scanning electron microscopy. Fig. 3a–c shows HUVECs attached to the wrinkled DLC film on the grooved PDMS substrate pre-treated with Ar plasma for t = 1 min. The cells spanned multiple microgrooves and tended to align along their direction (Fig. 3a). Closer observations reveal that the

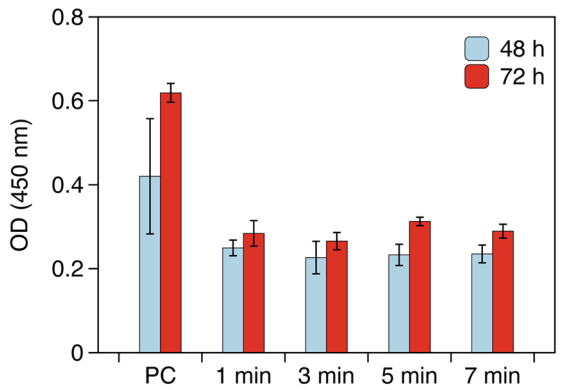

Fig. 2 Viability of HUVECs cultured on the sample surfaces. Optical density (OD) of the reaction mixture in the wells measured at 450 nm at periods of 48 and 72 hours of culture. PC denotes the positive control. The times indicate the durations of Ar plasma treatment performed prior to the deposition of DLC films.

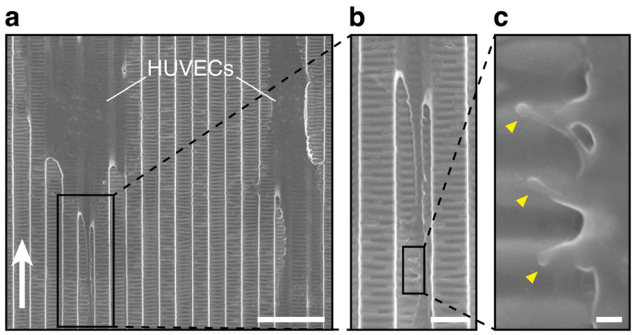

Fig. 3 (a–c) SEM images of HUVECs attached to the wrinkled DLC film on the grooved PDMS substrate that had been pre-treated with Ar plasma for t = 1 min. The white arrow in (a) indicates the groove orientation. A magnified image of the area indicated by the orange box in (a) is presented in (b). A magnified image of the area indicated by the black box in (b) is shown in (c). The yellow triangles in (c) indicate the filopodia-like protrusions of the HUVECS, suggesting the preferential attachment to the apex of the wrinkles. Scale bars: (a) 20 μm, (b) 5 μm, (c) 500 nm.

lamellipodia and filopodia-like protrusions of the HUVECs preferentially attach to the crests of the wrinkles formed on the microgrooves (Fig. 3b and c). These results demonstrate that the hierarchical patterns offer synergistic effects on cell behavior: the microgrooves guide cell alignment and elongation, while the wrinkles provide focal adhesion sites.

Similar cell behavior was observed for HUVECs cultured on the hierarchical patterns with different wrinkle dimensions. Fig. 4a–c presents the cells on the wrinkled DLC film on the grooved PDMS substrate pre-treated with Ar plasma for t = 5 min. Filopodia-like protrusions were attached to the wrinkle crests, as indicated by the yellow triangles in Fig. 4a. At another region, lamellipodia of the HUVEC confined between the grooves were observed on the wrinkle crests (Fig. 4b and c). Such preferential attachment of lamellipodia and filopodia to wrinkle crests likely arises from restricted cellular contact with wrinkle troughs due to their height and spacing. However, no clear differences were observed among the various wrinkle dimensions examined, suggesting that the wrinkle size does not significantly affect lamellipodia and filopodia adhesion within the range tested in this study.

Lamellipodia are broad, sheet-like protrusions formed by branched actin networks that enable cell extension and adhesion maturation, while filopodia are slender protrusions driven by actin bundles that function as sensory structures for detecting topographic features. On the surfaces prepared with Ar plasma for t = 1 min, which have finer wrinkle dimensions, HUVECs predominantly extended filopodia along ridges to initiate focal adhesion, while coarser wrinkles created with Ar plasma for t = 5 min induced both lamellipodia spreading and filopodia probing. Given the identical surface chemistry and stiffness, these differences in protrusion types between the surfaces may arise from topography-specific mechanotransduction cues. Future work, including quantitative analyses of signaling pathways and dynamic imaging, will be needed to elucidate these mechanisms and provide insights into adhesion, migration, and proliferation dynamics on the wrinkled and grooved scaffolds.

To assess the potential influence of mechanical stiffness on cell behavior, it is important to consider the mechanical properties of the DLC film and PDMS substrates. DLC films generally have high Young's moduli, ranging from several tens to several hundreds of GPa depending on the deposition method and the resulting film structure.[28,29] Meanwhile, PDMS with a mixture ratio of 10 : 1 typically exhibits a Young's modulus of approximately 2 MPa.[30] This substantial difference in Young's modulus between the film and substrate suggests that DLC coating considerably enhances the effective stiffness of the PDMS surface region, while the underlying PDMS remains compliant. Prior studies have demonstrated that cells sense substrate stiffness at depths on the order of micrometers,[31,32] which far exceed the thickness of the DLC film used in the present study. Therefore, it is plausible that HUVECs cultured on our wrinkled and grooved surfaces primarily sense the mechanical properties of the underlying compliant PDMS substrate rather than the stiff DLC film itself. This combination of a stiff, protective DLC film and a compliant PDMS substrate may provide a favorable mechanical environment that supports endothelial adhesion and proliferation, while avoiding excessive rigidity that could impair biological integration. Quantifying the effective mechanical properties sensed at the cell–film–substrate interface represents an important direction for future research.

Taken together, these results suggest that wrinkle crests provide physical cues that are recognized by HUVECs as favorable sites for adhesion or migration. The combination of microgrooves and nanoscale wrinkles thus offers distinct and complementary roles: microgrooves guide cell alignment, while wrinkles create localized specific adhesion sites. This hierarchical design strategy offers a promising route for engineering biomaterial surfaces that promote endothelialization. Given the widespread biomedical applications of PDMS and DLC, these wrinkled and grooved surfaces offer a promising foundation for endothelialization. Their ability to combine structural guidance for cell orientation with nanoscale features for specific adhesion makes them promising for blood-contacting medical devices.

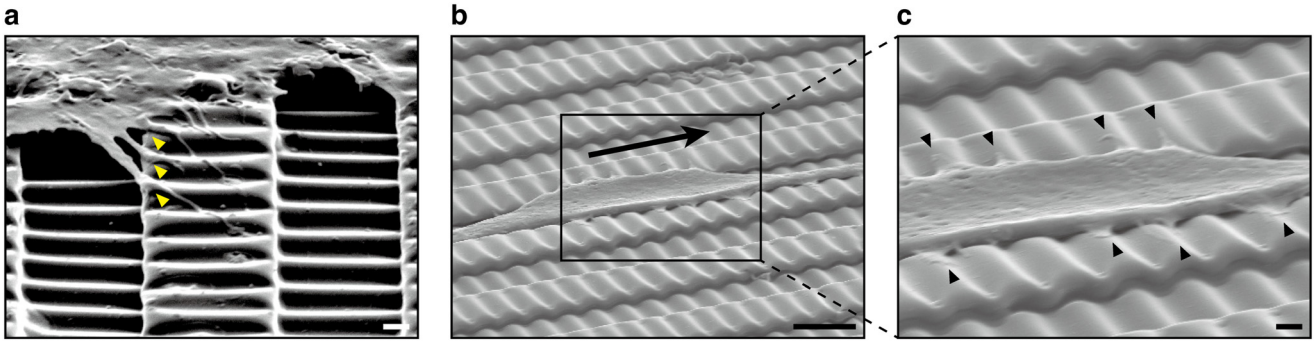

Fig. 4 HUVECs cultured on the hierarchical patterns. (a–c) Tilted SEM images of HUVECs on the wrinkled DLC film on the grooved PDMS substrate that had been pre-treated with Ar plasma for t = 5 min. The yellow triangles in (a) indicate the filopodia of the HUVECs. The black arrow in (b) indicates the groove direction. A magnified image of the area indicated by the black box in (b) is presented in (c). The black triangles in (c) indicate the locations to which the cells are attached. Scale bars: (a and b) 1 μm, (c) 5 μm.

Further investigations, including detailed analyses of protein adsorption and systematic optimization of groove and wrinkle dimensions, will be valuable for developing scaffolds that support stable endothelial layers and ensure long-term performance of vascular implants. Furthermore, chemically modified DLC films with enhanced biological properties could provide finer control over endothelial cell responses and expand the versatility of these hierarchical surfaces for regenerative medicine applications.[33–41]

Conclusions

HUVECs were cultured on wrinkled and grooved surfaces fabricated by exploiting surface instability of DLC-coated PDMS systems. SEM observations revealed that the cells elongated along the groove direction, while their lamellipodia and filopodia preferentially attached to the wrinkle crests. Because lamellipodia and filopodia play a key role in sensing, adhesion, and migration, controlling their interactions with surface topographies may provide a means to regulate vital cellular functions. Enzymatic assays further confirmed sustained cell viability and active proliferation across different wrinkle dimensions, demonstrating the cytocompatibility of these hierarchical surfaces. Taken together, the hierarchical patterns composed of wrinkled DLC films on microgrooved PDMS substrates presented in this study offer a promising approach for precise control of endothelial cell behavior, which is essential for fabricating optimally designed scaffolds in vascular tissue engineering.

Materials and methods

PDMS prepolymer was prepared by mixing a silicone elastomer base with a curing agent at a ratio of 10 : 1 by weight (Silpot 184, Dow Corning Toray Co., Ltd.) and cured at 70 °C for 120 min. Prior to curing, the air bubbles trapped in the mixture were removed in a vacuum chamber. PDMS substrates with parallel channels of equal groove and ridge with a width of 5 μm and a depth of 1 μm were fabricated by a molding method using a grooved SiO_2 master on Si wafer. The grooved surfaces of the PDMS substrates were treated with Ar plasma for varying durations t, followed by deposition of DLC film with a radio frequency plasma-enhanced chemical vapor deposition apparatus (Custom-built, Hirano Koh-on Co., Ltd.) with a frequency of 13.56 MHz. The Ar plasma treatment was carried out for 1 to 7 min at a power of 200 W and a pressure of 26.6 Pa. The DLC film was subsequently deposited onto the surface from acetylene (C_2H_2) gas. The deposition was performed for 10 s at a power of 200 W and a pressure of 13.3 Pa. The film thickness was approximately 40 nm, as measured with a profilometer (Dektak 3030, Veeco Instruments Inc.).

The samples were placed in 48-well plates and then sterilized using ethylene oxide gas. The wells used for positive control were coated with 0.1% gelatin for a given period in a humidified 5% CO_2 incubator at 37 °C prior to cell seeding to enhance the cell adhesion. Afterwards, the gelatin solution in the wells was aspirated and the wells were washed with phosphate-buffered saline without calcium and magnesium. The samples were then incubated with the HUVECs in the incubator. In particular, HUVECs at passage 4 in endothelial basal medium (EBM-2, Lonza) supplemented with endothelial growth factor (EGM-2, Lonza) were seeded on the sample surfaces and the gelatin-coated wells at a density of approximately 4.6×10^4 cells per mL, and the plates were placed in the incubator. The viability of the HUVECs was assessed by measuring the enzymatic activity using Cell Counting Kit-8 (WST-8 assay kit, Dojindo Molecular Technologies). After prescribed periods, the plates were removed from the incubator, and the medium in each well was replaced with 500 μL of RPMI medium (Lonza) containing 50 μL of Cell Counting Kit-8. The plates were then returned to and placed in the incubator for approximately 90 min. Thereafter, 100 μL of the reaction mixture in each well was transferred to a 96-well plate, and the optical density at 450 nm was measured with a microplate reader (Microplate Reader, EZS ABS, Iwaki Asahi Technoglass). The results are expressed as the mean of 3 replicates and the corresponding standard deviation.

The HUVECs attached to the wrinkled and grooved surfaces were observed under a scanning electron microscope (SEM, Sirion, FEI Company) operated at an accelerating voltage of 5 kV. For the SEM observation, the reaction mixture for WST-8 assay in each well was aspirated, and the HUVECs attached to the wrinkled and grooved surfaces were subsequently fixed in 2.5% glutaraldehyde overnight. After fixation, the samples were dehydrated in a graded ethanol series (40, 60, 80, and 99.5% for 15 min each). The samples were then coated with osmium to prevent electron charging.

Author contributions

So Nagashima: conceptualization, visualization, methodology, writing – original draft. Terumitsu Hasebe: supervision, funding acquisition, writing – review & editing. Atsushi Hotta: writing – review & editing. Tetsuya Suzuki: writing – review & editing.

Conflicts of interest

There are no conflicts to declare.

Data availability

The data that support the findings of this study are available within the article. Additional experimental data are available from the corresponding author upon reasonable request.

Acknowledgements

We greatly appreciate the expertise of Noriko Kitamura and Fusako Watanabe of the Toho University Sakura Medical Center on the cell culture experiments. This work was supported in

part by a Grant-in-Aid for the Global Center of Excellence Program for the "Center for Education and Research of Symbiotic, Safe and Secure System Design" (S. N. and A. H.) and a Grant-in-Aid for Young Scientists (B) from JSPS (No. 21760561 to T. H.). This paper is dedicated to the memory of our colleague and friend, Yukihiro Yoshimoto, whose inspiration and contributions have left a lasting impact on our work.

References

1 J. Zhang, K. Ren, J. Qiu, B. Chen, W. Duan, J. Liu, G. Li and D. Li, *Mater. Today Bio*, 2024, **25**, 100968.
2 O. Bjorgvinsdottir, S. J. Ferguson, B. S. Snorradottir, T. Gudjonsson and K. Wuertz-Kozak, *Mater. Today Bio*, 2024, **26**, 101060.
3 A. A. Conner, D. David and E. K. Yim, *Adv. Healthcare Mater.*, 2024, **13**, 2400335.
4 C. F. Natale, J. Lafaurie-Janvore, M. Ventre, A. Babataheri and A. I. Barakat, *J. R. Soc., Interface*, 2019, **16**, 20190263.
5 T. Govindarajan and R. Shandas, *ACS Appl. Bio Mater.*, 2019, **2**, 1897–1906.
6 C. Leclech and C. Villard, *Front. Bioeng. Biotechnol.*, 2020, **8**, 551505.
7 C. Leclech, D. Gonzalez-Rodriguez, A. Villedieu, T. Lok, A.-M. Déplanche and P. Silberzan, *Nat. Commun.*, 2022, **13**, 2797.
8 C. Leclech, G. Cardillo, B. Roellinger, X. Zhang, J. Frederick, K. Mamchaoui, C. Coirault and A. I. Barakat, *Adv. Sci.*, 2025, **12**, 2410052.
9 L. Liu, J. Wu, S. Lv, D. Xu, S. Li, W. Hou, C. Wang and D. Yu, *Mater. Today Bio*, 2023, **23**, 100866.
10 F. Tian, L. Yin, P. Lin, Y. Liu, W. Wang, Y. Chen and Y. Tang, *ACS Appl. Mater. Interfaces*, 2023, **15**, 17518–17531.
11 R. Zhang, M. Zhu, Y. Liu, L. Hu, P. Chen, J. Wang, B. Tang, C. Liu and F. Ren, *ACS Appl. Mater. Interfaces*, 2025, **17**, 41765–41780.
12 J. Kim, S. Nagashima, J. Wang, S. Matsubara, E. Maeda, D. Okumura and T. Matsumoto, *Proc. Inst. Mech. Eng., Part H*, 2025, **239**, 1000–1009.
13 C. A. Dessalles, C. Leclech, A. Castagnino and A. I. Barakat, *Commun. Biol.*, 2021, **4**, 764.
14 R. K. Roy and K.-R. Lee, *J. Biomed. Mater. Res., Part B*, 2007, **83**, 72–84.
15 R. Asakawa, S. Nagashima, Y. Nakamura, T. Hasebe, T. Suzuki and A. Hotta, *Surf. Coat. Technol.*, 2011, **206**, 676–685.
16 T.-J. Ko, E. Kim, S. Nagashima, K. H. Oh, K.-R. Lee, S. Kim and M.-W. Moon, *Soft Matter*, 2013, **9**, 8705–8711.
17 Y. Yoshimoto, T. Hasebe, K. Takahashi, M. Amari, S. Nagashima, A. Kamijo, A. Hotta, K. Takahashi and T. Suzuki, *Microsc. Res. Tech.*, 2013, **76**, 342–349.
18 S. Nagashima, M.-W. Moon and K.-R. Lee, in *Diamond-Like Carbon Coatings for Joint Arthroplasty*, ed. R. Sonntag and J. P. Kretzer, Imperial College Press, London, 2015, pp. 395–412.
19 S. Nagashima and M.-W. Moon, in *Diamond-Like Carbon Coatings with Special Wettability for Automotive Applications*, ed. S. C. Cha and A. Erdemir, Springer International Publishing, Switzerland, 2015, pp. 191–202.
20 X. Ma, Q. Zhang, P. Guo, X. Tong, Y. Zhao and A. Wang, *ACS Appl. Mater. Interfaces*, 2020, **12**, 45549–45557.
21 M. J. Hoque, L. Li, J. Ma, H. Cha, S. Sett, X. Yan, K. F. Rabbi, J. Y. Ho, S. Khodakarami, J. Suwala, W. Yang, O. Mohammadmoradi, G. O. Ince and N. Miljkovic, *Nat. Commun.*, 2023, **14**, 4902.
22 M. Birkett, A. W. Zia, D. K. Devarajan, Soni, M. I. Panayiotidis, T. J. Joyce, M. M. Tambuwala and Á. Serrano-Aroca, *Acta Biomater.*, 2023, **167**, 54–68.
23 R. Shah, N. Pai, R. Khandekar, R. Aslam, Q. Wang, Z. Yan and A. Rosenkranz, *Surf. Coat. Technol.*, 2024, **487**, 131006.
24 Sk. F. Ahmed, S. Nagashima, J. Y. Lee, K.-R. Lee, K.-S. Kim and M.-W. Moon, *Carbon*, 2014, **76**, 105–112.
25 S. Nagashima, T. Hasebe, A. Hotta and T. Suzuki, *Diamond Relat. Mater.*, 2025, **151**, 111855.
26 S. Nagashima, T. Hasebe, D. Tsuya, T. Horikoshi, M. Ochiai, S. Tanigawa, Y. Koide, A. Hotta and T. Suzuki, *Diamond Relat. Mater.*, 2012, **22**, 48–51.
27 N. Bowden, W. T. S. Huck, K. E. Paul and G. M. Whitesides, *Appl. Phys. Lett.*, 1999, **75**, 2557–2559.
28 J. Robertson, *Diamond Relat. Mater.*, 1992, **1**, 397–406.
29 T. A. Amollo, K. Wang, N. Baule, L. Haubold and Q. H. Fan, *Diamond Relat. Mater.*, 2025, **154**, 112138.
30 D. M. Kingsley, C. H. McCleery, C. D. Johnson, M. T. Bramson, D. Rende, R. J. Gilbert and D. T. Corr, *J. Mech. Behav. Biomed. Mater.*, 2019, **92**, 152–161.
31 I. Schoen, B. L. Pruitt and V. Vogel, *Annu. Rev. Mater. Res.*, 2013, **43**, 589–618.
32 P. A. Janmey, D. A. Fletcher and C. A. Reinhart-King, *Physiol. Rev.*, 2020, **100**, 695–724.
33 T. Hasebe, S. Nagashima, A. Kamijo, T. Yoshimura, T. Ishimaru, Y. Yoshimoto, S. Yohena, H. Kodama, A. Hotta, K. Takahashi and T. Suzuki, *Thin Solid Films*, 2007, **516**, 299–303.
34 R. Roy, H. Choi, J. Yi, M.-W. Moon, K.-R. Lee, D. Han, J. Shin, A. Kamijo and T. Hasebe, *Acta Biomater.*, 2009, **5**, 249–256.
35 S. Nagashima, T. Hasebe, A. Kamijo, Y. Yoshimoto, A. Hotta, H. Morita, H. Terada, M. Tanaka, K. Takahashi and T. Suzuki, *Diamond Relat. Mater.*, 2010, **19**, 861–865.
36 Y. Yoshimoto, T. Hasebe, S. Nagashima, A. Kamijo, T. Nakatani, T. Yamagami, N. Kitamura, T. Kitagawa, A. Hotta, K. Takahashi and T. Suzuki, *Jpn. J. Appl. Phys.*, 2012, **51**, 090129.
37 T. Hasebe, S. Nagashima, A. Kamijo, M.-W. Moon, Y. Kashiwagi, A. Hotta, K.-R. Lee, K. Takahashi, T. Yamagami and T. Suzuki, *Diamond Relat. Mater.*, 2013, **38**, 14–18.
38 S. Maegawa, T. Hasebe, Y. Yamato, K. Bito, S. Nagashima, T. Hayashi, T. Mine, T. Matsumoto, A. Hotta and T. Suzuki, *Diamond Relat. Mater.*, 2016, **70**, 33–38.
39 M. Zhang, T. Xie, X. Qian, Y. Zhu and X. Liu, *ACS Omega*, 2020, **5**, 22772–22777.
40 M. Toyonaga, T. Hasebe, S. Maegawa, T. Matsumoto, A. Hotta and T. Suzuki, *Diamond Relat. Mater.*, 2021, **119**, 108558.
41 X. Wei, Y. Zhang, H. Feng, X. Cao, Q. Ding, Z. Lu and G. Zhang, *ACS Biomater. Sci. Eng.*, 2022, **8**, 1166–1180.